# A STUDY ON THE YEARLONG RECORD OF SOUND PROPAGATION FROM THE CANADA BASIN TO THE CHUKCHI SHELF MEASURED ON A HORIZONTAL LINE ARRAY

Megan S. Ballard[a], Mohsen Badiey[b], Jason D. Sagers[a], John A. Colosi[c], Altan Turgut[d], Sean Pecknold[e], Ying-Tsong Lin[f], Andrey Proshutinsky[f], Richard Krishfield[f], Peter F. Worcester[g], and Matthew A. Dzieciuch[g]

[a]Appl. Res. Labs., Univ. of Texas at Austin, Austin, TX, USA
[b]University of Delaware, Newark, DE, 19716, USA
[c]Naval Postgrad. School, Monterey, CA, USA USA
[d]U.S. Naval Research Laboratory, Washington, DC, USA
[e]Defence Research and Development Canada, Dartmouth, Nova Scotia, Canada
[f]Woods Hole Oceanographic Institution, Woods Hole, MA, USA
[g]Scripps Institution of Oceanography, University of California at San Diego USA

***Abstract:*** *The Pacific Arctic Region has experienced decadal changes in atmospheric conditions, seasonal sea-ice coverage, and thermohaline structure. From September 2016 to October 2017, the Canada Basin Acoustic Propagation Experiment (CANAPE) was conducted to observe the changing soundscape and to explore the use of acoustic remote sensing techniques in the transitioning Arctic. During the experiment, low-frequency signals from five tomographic sources located in the Canada Basin were recorded by an array of hydrophones with both horizontal and vertical apertures located on the Chukchi Shelf at the 150 m isobath. The propagation distances ranged from 240 km to 520 km, and the propagation conditions changed from persistently ducted in the basin to seasonally upward refracting on the continental shelf. An analysis of the received level from the tomography sources revealed a spatial dependence in the onset of the seasonal increase in transmission loss, which was correlated with the locations of the sources in the basin. This observation led to the hypothesis that the water advected from Barrow Canyon westward over the continental slope by the Chukchi slope current contributes to the temporal and spatial dependence observed in the acoustic record. The water column properties and ice draft were measured by oceanographic sensors on the basin tomography moorings and by six vertical arrays of oceanographic moorings on the continental shelf to characterize the temporal and spatial variability of the environment. This talk examines the range-dependent measurements and seeks to explain the observed variability in the received signals through propagation modeling.*


***Keywords:*** *Arctic Oceanography, Sea Ice, Beaufort Gyre, Chukchi Shelf*

## 1. INTRODUCTION

The Pacific Arctic Region has experienced decadal changes in atmospheric conditions, seasonal sea-ice coverage, and thermohaline structure. Sea-ice losses in the northern Chukchi and Beaufort Seas during the summer melt season have resulted in an increase in the ice-free ocean area of 70% compared to the climatological mean [1]. Furthermore, a doubling in Beaufort Gyre halocline heat content has been observed over the past three decades [2]. Both of these changes have implications for acoustic propagation: sound incurs less surface loss from open water than from the rough ice interface, and it is more efficiently channeled by warmer water in the upper halocline which forms the top boundary of an acoustic duct.

The Canada Basin Acoustic Propagation Experiment (CANAPE) was conducted over a yearlong period beginning in September 2016. The experiment objectives were to understand the changing soundscape and to explore the use of acoustic signals as a remote sensing tool in the transitioning Arctic. During the experiment, low-frequency signals from five Scripps Institution of Oceanography (SIO) tomographic sources located in the Canada Basin were recorded by the Applied Research Laboratories at the University of Texas at Austin (ARL:UT) PErsistent aCoustic Observation System (PECOS) array of hydrophones located on the Chukchi Shelf. The locations of the SIO sources and the PECOS array are shown in Fig. 1.

To support the acoustic propagation experiment, environmental measurements were made in the Canada Basin and on the Chukchi Shelf. The locations of environmental measurements are indicated by triangles in Fig. 1. Water temperature and salinity were measured in the basin by the SIO deep vertical line array (DVLA) and on the shelf by the University of Delaware (UDel) array of oceanographic moorings (OM). An additional set of oceanographic measurements in the basin were obtained by the Beaufort Gyre Exploration Project (BGEP) [3,4]. Collectively, these data indicate that the range-dependent propagation conditions change from predominately ducted in the basin to seasonally upward refracting on the continental shelf. Ice draft was measured in both locations by Upward Looking Sonars (ULS). In the basin, each of the SIO tomography moorings included an ULS, and on the shelf, ice draft was measured by the Naval Research Laboratory (NRL) ULS. This paper examines the temporal changes of the

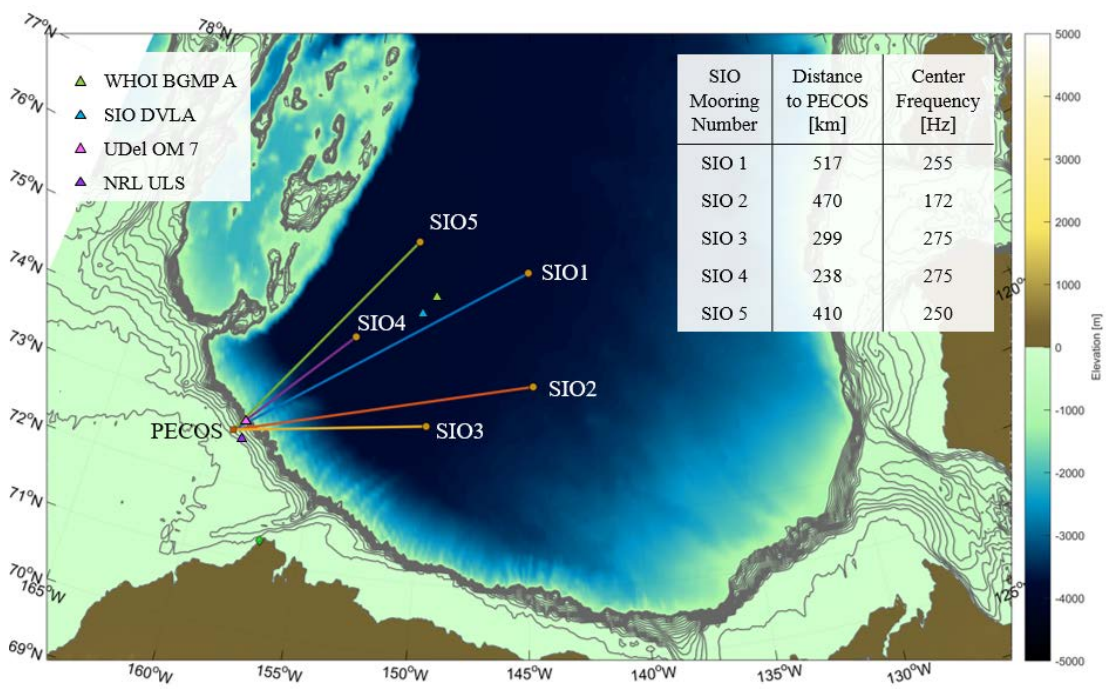


| SIO Mooring Number | Distance to PECOS [km] | Center Frequency [Hz] |
|---|---|---|
| SIO 1 | 517 | 255 |
| SIO 2 | 470 | 172 |
| SIO 3 | 299 | 275 |
| SIO 4 | 238 | 275 |
| SIO 5 | 410 | 250 |

*Fig.1: Map of CANAPE, including the locations of acoustic sources (circles), receiver (square), and environmental measurements (triangles). The propagation paths from the SIO sources in the basin to the PECOS receiver array on the shelf are illustrated by the colored lines.*

range-dependent measurements and explains the observed variability in the received level (RL) of the acoustic signals through propagation modeling.

## 2. ACOUSTIC MEASUREMENTS

The SIO tomography sources in the Canada Basin broadcast 135 s-long linear frequency modulated (LFM) signals. The sources were scheduled to broadcast sequentially at 6 min. intervals once every four hours. The signals had 100 Hz bandwidth, and the center frequencies are listed in the embedded table in Fig. 1. The sources were deployed at a nominal depth of 175 m, so that they were located in the sound speed duct.

The signals were measured by the horizontal line array (HLA) and recorded by PECOS. The 34-element HLA was designed as a 220 m-long center-tapered array, and the data were recorded at a sampling rate of 8192 Hz. The measured signals were pulse compressed and conventional frequency-domain beamforming was applied using 0.5 s integration time with 75% overlap. The transmission loss (TL) for each reception was determined by subtracting the peak RL (calculated from the pulse-compressed beamformed time series) from the known source level (SL). Relative TL was calculated by normalizing TL throughout the year such that the average TL during the open-water condition in August was equal to zero.

Relative TL from all five SIO tomography sources is shown in Fig. 2. Receptions from all five moorings display the seasonal increase in TL during the fall and winter, and a decrease in TL in the summer. However, the onset of the increase/decrease in TL appears correlated with position. Receptions from the most eastern moorings experience the change in propagation conditions more than a month before the receptions from the western most moorings. Additionally, the rate of decrease in TL appears faster for the western moorings. For receptions from all sources, TL temporarily decreases for periods between April and June. There are also periods for which the ambient noise level exceeded the RL; relative TL is not reported for these periods.

## 3. ENVIRONMENTAL MEASUREMENTS

The top panel of Fig. 3 shows the daily mean ice draft measured by the ULS in the basin and on the shelf. The ULS measurements were made on all five SIO source moorings, but are missing for periods when currents on the mooring line pulled the ULS away from the ice canopy. The NRL ULS on the shelf stopped recording in the beginning of February. For all

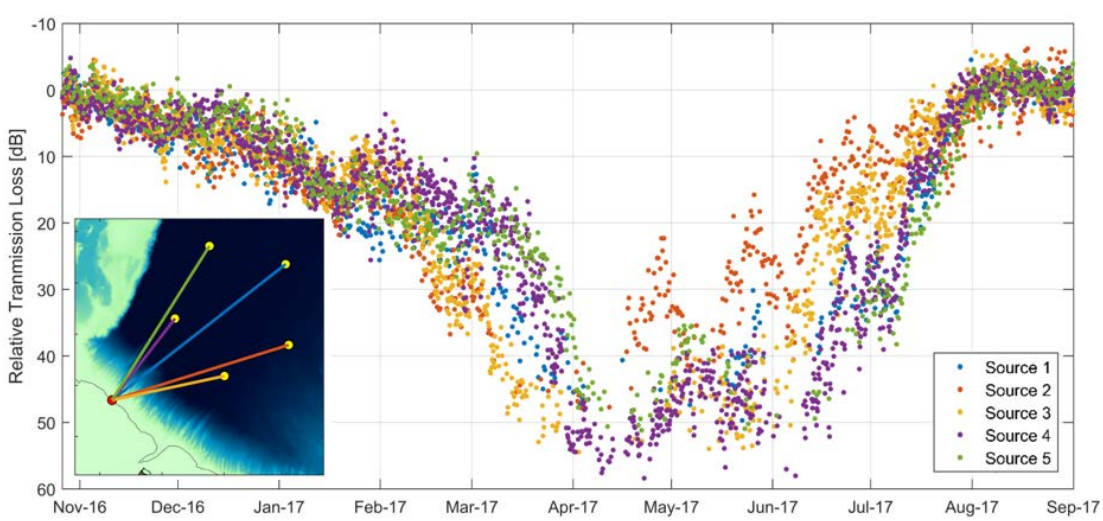


*Fig.2: Relative TL of receptions from the SIO tomography sources recorded on PECOS. The inset map shows the acoustic paths from the SIO moorings to the PECOS array.*

moorings, a gradual increase in ice thickness is observed between November and April, at which time the ice reaches its maximum daily mean thickness of 1.5 m to 2 m. After mid-June, the ice begins to melt, and the mean ice draft rapidly decreases.

The lower panel of Fig. 3 shows seawater temperature representative of the water masses in the halocline that form the sound speed duct. The Pacific summer water (PSW), which forms the upper boundary of the acoustic duct, is warmer and less saline and consequently overlies the cooler Pacific winter water (PWW), which forms the sound speed minimum in the duct. For each of the three measurement locations shown in Fig. 3, the temperature of the PSW was calculated as the maximum temperature in the upper 150 m of the water column, and the PWW was calculated as the minimum temperature between 100 and 200 m depth.

Within the Beaufort Gyre, the temperatures of the PSW and PWW were relatively constant over the yearlong measurement period. The PSW is consistently warmer than -0.5ºC; the anomalous values in early May in the DVLA measurements are caused by movement of the mooring line that pulled the sensors below the depth of the PSW layer. The observed variability in the PSW in the Canada Basin is due to in situ mixing and changes in source-water properties. The PWW shows even less variability with persistent temperatures around -1.5 ºC. These data indicate the ducted sound propagation conditions are present in the Beaufort Gyre throughout the yearlong measurement period.

In contrast, the temperatures measured on the shelf show considerably more seasonal variability. On the Chukchi Shelf, it is typical to further subdivide the Pacific water masses into a greater number of categories depending on their temperature and salinity [5-8]. The present analysis does not make this discrimination, as the larger focus of this study is on determining the presence of an acoustic duct. As shown in the lower panel of Fig. 3, the maximum temperature in the upper 150 m measured by UDel OM 7 exceeds 1ºC for the open water period in summer as well as in the fall and early winter. Beginning in January, the maximum temperature begins to decrease, with the most dramatic decrease in temperature occurring in February and March. The maximum temperature on the shelf remains lower than the temperature of the PSW in the basin until the breakup of the ice cover in early July. Similarly, more variability is observed in the minimum sound speed on the slope compared to the PWW

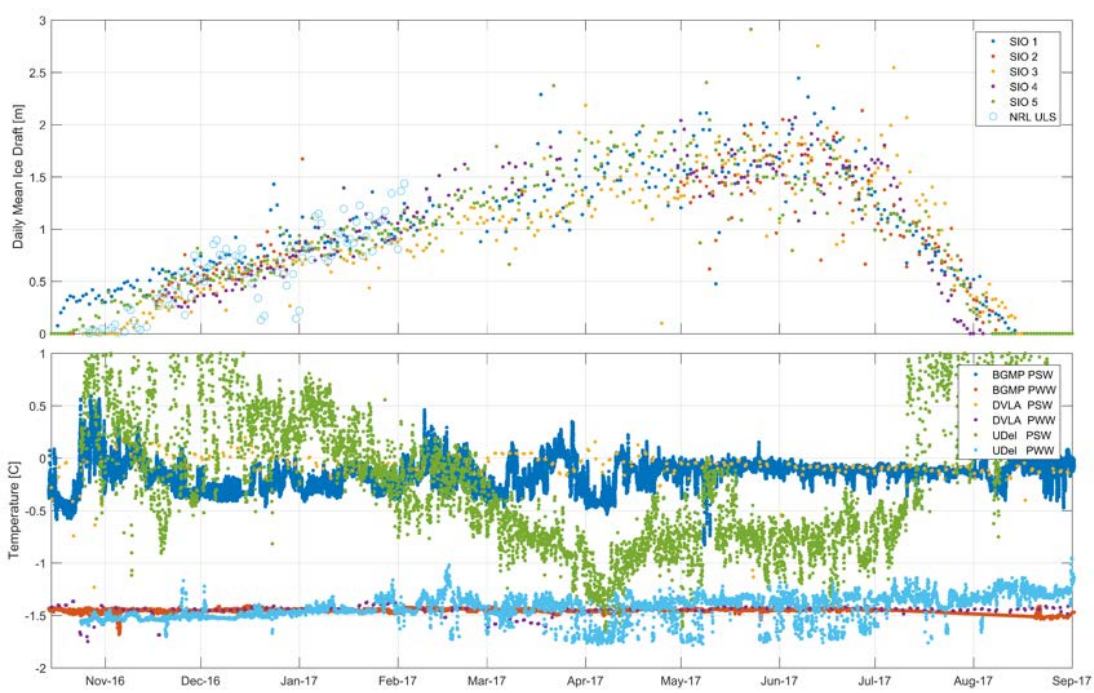


*Fig.3: Top panel: Daily mean ice draft calculated from measurements of ULS on each of the SIO moorings in the basin and the NRL mooring the shelf. Bottom panel: Temperature of the upper boundary of the acoustic duct in the basin and on the shelf.*

in the basin. These measurements indicate the acoustic duct is present on the Chukchi Shelf in the summer and fall, but weakens and/or dissipates in the winter and spring. The influx of colder water in the upper 150 m observed in the UDel OM 7 measurements is believed to be transported by the Chukchi slope current. The Chukchi slope current transports Pacific-origin water westward over the continental slope [5]. The volume of water transported and speed of its flow change throughout the course of the year [6-8].

Comparison of the relative TL to the environmental measurements reveals some potential relationships between the data sets. For example, the increase in TL that occurs in February and March appears correlated with the decrease in the maximum temperature on the shelf. The decrease in relative TL between mid-June and August appears correlated with the melting ice cover as indicated by the decrease in the daily mean ice draft. Although these observations may lend some understanding into the environmental effects on TL, the true propagation conditions are simultaneously influenced by both the presence of the ice cover, which causes increased loss due to surface scattering, and the water column properties, which can insulate the acoustic field from surface loss when the sound speed profile is downward refracting. To investigate the interrelationship between these effects, acoustic propagation modeling was carried out using the environmental measurements.

## 4. ACOUSTIC PROPAGATION MODELING

Transmission loss from the SIO sources in the basin to the PECOS array on the shelf was modeled using the ray model BELLHOP [9]. The ray theory is an approximate solution to the wave equation, and this modeling approach was chosen for its efficiency. In this application, there are inaccuracies related to the frequency-dependent extent to which sound is trapped in the sound speed duct. The ray solution includes rays that are fully trapped within the duct that do not incur surface loss. However, the low-frequency SIO source signals are not fully trapped in the duct, and accumulate loss as they propagate through the Beaufort Sea. Additionally, the environmental measurements between deep and shallow water sites are sparse and temporally and spatially under-sampled. Despite these shortcomings, the model reproduces the seasonal changes in TL studied in this paper.

Surface loss was calculated using an empirical model derived from historical data based loosely on Ref. 10. The only inputs to the model are the root-mean-square value of the ice draft $\sigma$, which was calculated from the ULS on the SIO moorings, and the center frequency of the source signals. By ony using ULS data from the source location, constant ice draft statistics are assumed over the entire propagation path. The reflection coefficient $R$ in dB is calculated by

$$\begin{aligned} R(\sigma, f) &= 0.00190 f (2\sigma)^{1.5} \qquad & f \leq 403(2\sigma)^{-0.5} \\ R(\sigma, f) &= 0.541(2\sigma)^{1.5} \qquad & f > 403(2\sigma)^{-0.5} \,. \end{aligned} \tag{1}$$

This surface loss model does not account for dependence on sea ice thickness, properties, spatial correlation length of the roughness, and other characteristics that are important in determining the reflection coefficient. To account for variable sea ice coverage over the acoustic propagation path, the sea ice concentration was taken into account using the MASIE-AMSR2 (MASAM2) database [11]. For seasonal periods of ice growth in October and November and ice melt in June and July, the reflection coefficient calculated from Eq. (1) was weighted by the range-dependent ice concentration along the propagation path.

For each eight-hour period of the yearlong experiment, the range- and depth-dependent water-column sound-speed field was constructed using measurements from the BGEP and the UDel OM array. The two-dimensional sound-speed field was divided into four domains which were each informed by different data sets or interpolation schemes. An example of the water-column sound-speed field for April 1, 2017 with the different domains labeled is shown in

Fig. 4. The boundary between the regime of ducted propagation in the basin and seasonally upward refracting propagation in the slope was defined to be 100 km offshore [5].

The first domain is characterized by ducted sound propagation and is made up of data measured by BGEP Mooring A. Range-dependent sound-speed profiles were derived from the temporal measurements by advecting the measured profile in space using the average Beaufort Gyre speed of 0.02 m/s. The sound speed in the second domain was constructed using the temporally relevant measurement from each of the UDel OM. The locations of the UDel OM are indicated by the white triangles above the plot. The third domain is defined as the upper 140 m of the water column offshore of the UDel OM array. Within domains two and three, the sound speed profile is expected to show strong seasonal dependence influenced by the water masses advected by the slope current. Since no direct measurements were made within region three, the water column properties were extrapolated from the northernmost mooring of the UDel OM array. For the five locations marked by the black triangles in Fig. 4, the median sound speed for a 24-hour period immediately following the signal transmission was used. To simulate range-dependence within this region, the sound speed profile for each marker location was calculated from different interleaving 5-hour blocks with the 24-hour period. A 2D interpolation was used for the fourth domain to accommodate the change in the depth of the Atlantic water layer between the measurements in basin and on the shelf. Finally, all the profiles were interpolated onto a 1 km grid for use in BELLHOP.

To account for the advection of PWW by the Chukchi slope current, the water-column properties making up domains two and three were temporally shifted to account for the lag in the seasonal increase in TL. Recalling the experiment geometry in Fig. 1, the propagation paths are spread over the slope so that water from the westward flowing slope current reaches the propagation path from SIO 3 first, followed by the paths from SIO 2, SIO1, SIO 4, and SIO 5. The estimates for the lag times were obtained from an examination of the increase in the relative TL during February and March shown in Fig. 2. For the propagation path from SIO 1 to PECOS, which is perpendicular to the shelf break, no temporal shift was applied. For the propagation paths from SIO 2 and SIO 3, which are located to the east of the SIO 1 propagation path, temporal shifts of -16 days and -23 days were applied. For the propagation paths from SIO 4 and SIO 5, which are located to the west of the SIO propagation path, temporal shifts of 6 days and 12 days were applied. The application of a uniform temporal shift to the 2D sound speed field is a coarse approximation of the advection of water by the slope current. A more accurate representation would account for the orientation of the propagation paths oblique to the shelf break as well as the seasonal variation in the speed of the current.

The BELLHOP model produces a set of arrivals, each described by a complex amplitude and travel time. The time-domain representation for the received waveform was calculated through application of the convolution theorem [12]. A short-time Fourier transform with 0.5 s time

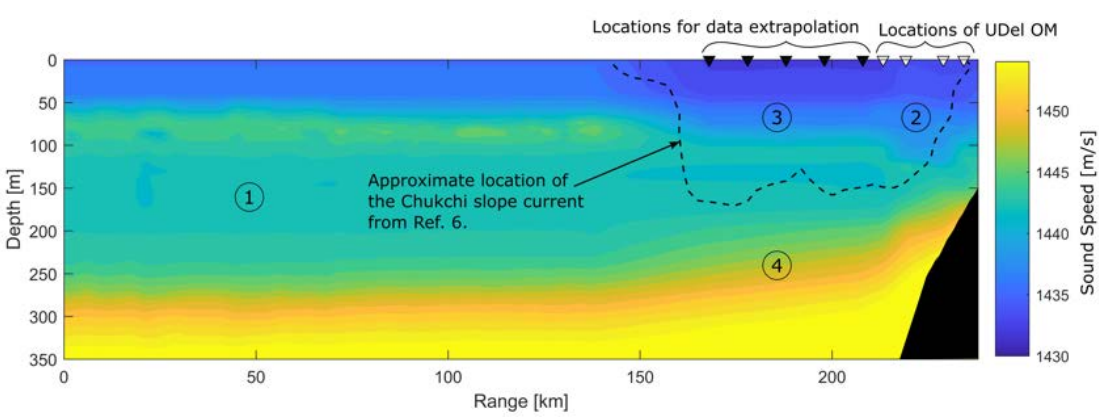


*Fig. 4: Water-column sound-speed field constructed for April 1, 2017. The numbered markers represent regions informed by different data sets and/or interpolations.*

window and 75% overlap was applied to the calculated time series for comparison with the measured data, which were beamformed in the frequency domain using 0.5 s integration time.

A comparison of the measured and modeled peak RL is shown in Fig. 5. Two calculations of the modeled RL are shown: one that accounts advection of the PWW by the slope current using the temporal shifts described above, and another that neglects the temporal shifts. For both calculations, there are times throughout the year when the model overestimates/ underestimates TL. The discrepancies between measured and modeled RL can be attributed to both approximations in the environmental model and the acoustic propagation model. There are also distinct periods where the modeled RL is lower than the 20 dB limit of the plot (i.e., mid-Feb. to mid-Apr. for SIO 2, and late Mar. to late Apr. for SIO 4). These periods correspond to times when currents pulled the mooring cable down so that the source was no longer in the sound speed duct.

For propagation from SIO 1 to PECOS, no temporal shift was applied for either modeled case since the propagation path is perpendicular to the shelf break. Comparision with the measured data shows good agreement in both the timing and magnitude of the seasonal increase and decrease in TL. For SIO 2 and SIO 4, the depth of the source influences the increase in TL in February and March, and the effects of the advection by the slope current cannot be readily observed. Comparisons of the two calculations of RL with the measured data for SIO 3 and SIO 5 most clearly show the impact of the advection of PWW over the slope. For SIO 3, calculation that neglects the temporal shift, the seasonal increase in TL occurs approximately three weeks late, and for SIO 5, it occurs almost two weeks early. Conversely, the solutions that include the temporal shifts agree with the measured data. These results support the hypothesis that the increase in TL February and March is caused by the advection of cold water by the slope current, which produces an upward refracting sound speed profile over the shelf.

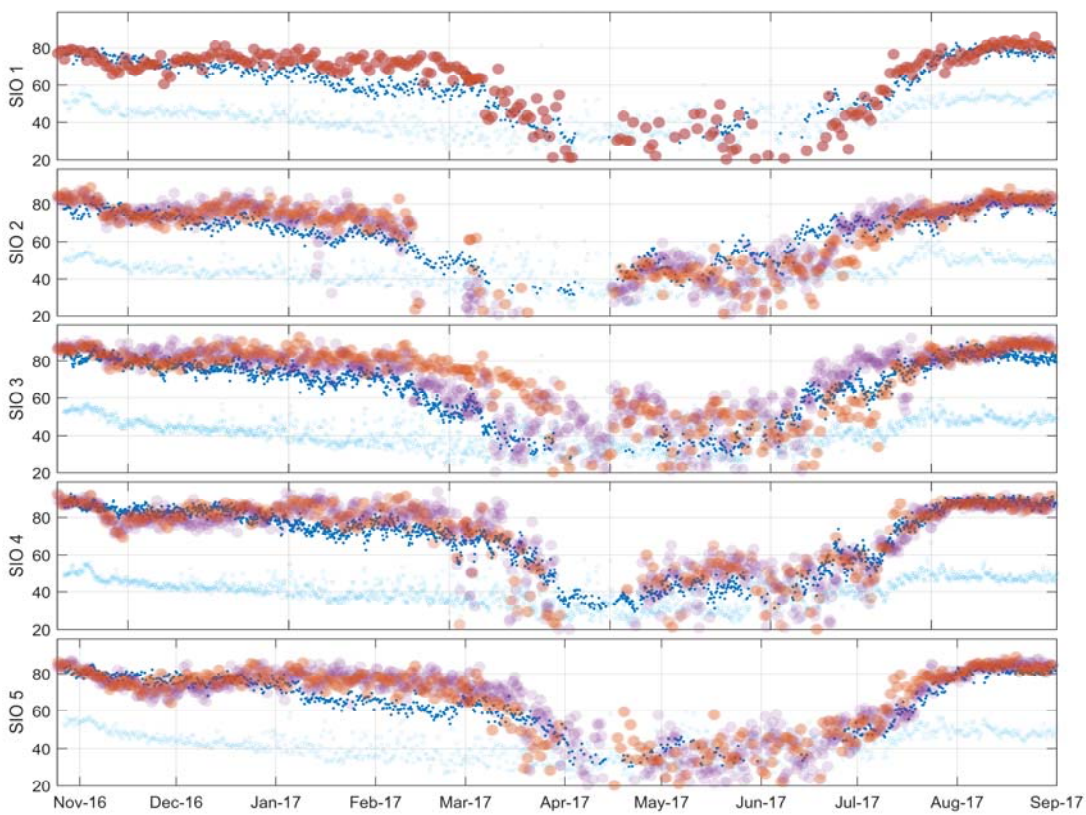


*Fig.5: Peak RL for the measured and modeled signals from the five SIO moorings to the PECOS array. The measured RL (dark blue dots), and the measured background noise (light blue dots). The modeled RL are shown by the including the temporal shift to account for advection of water by the Chukchi slope current (purple dots) and neglecting the temporal shift (orange dots).*

## 5. CONCLUSIONS

The measurements of long-range acoustic propagation from the Canada Basin to the Chukchi Shelf show a seasonal pattern of TL believed to be related to the outflow of the Chukchi slope current and the ice cover. The increase in TL in the winter was hypothesized to be caused by the advection of cold water by the Chukchi slope current westward, which resulted in an upward refracting sound speed profile leading to increased surface loss over this portion of the propagation path. The decrease in TL in the summer was associated with breakup of the ice cover, which exposed the eastern mooring locations to open water conditions first. These interpretations were supported by results from a ray-based acoustic propagation model that provided good agreement in both the timing and magnitude of the seasonal changes in TL. However, the modeling involved a number of assumptions, including extrapolation of the oceanographic data and simplified modeling of the surface loss from the ice cover. A physics based, coupled ice-ocean model of this region can improve reconstruction of time and range dependent environmental input parameters.

## 6. ACKNOWLEDGEMENTS

This work was sponsored by the Office of Naval Research under Grant Numbers N00014-15-1-2144, N00014-15-1-2119, N00014-15-1-2017, N00014-15-1-2068, N00014-15-1-2110, and N00014-15-1-2898.

## REFERENCES

[1] K. R. Wood, N. A. Bond, S. L. Danielson, J. E. Overland, S. A. Salo, P. J. Stabeno, and J. Whitefield, “A decade of environmental change in the pacific arctic region,” Prog Oceanogr. 136, 12–31, 2015.
[2] M. L. Timmermans, J. Toole, R. Krishfield, “Warming of the interior Arctic Ocean linked to sea ice losses at the basin margins,” Sci. Adv., 2018.
[3] http://www.whoi.edu/beaufortgyre
[4] R. A. Krishfield, A. Proshutinsky, K. Tateyama, W. J. Williams, E. C. Carmack, F. A.McLaughlin, and M. L. Timmermans, “Deterioration of perennial sea ice in the beaufort gyre from 2003 to 2012 and its impact on the oceanic freshwater cycle,” J. Geophys. Res. Oceans 119, 1271–1305, 2014.
[5] W. B. Corlett and R. S. Pickart, “The Chukchi slope current,” Prog Oceanogr. 153, 2017.
[6] M. A. Spall, R. S. Pickart, M. Li, M. Itoh, P. Lin, T. Kikuchi, and Y. Qi, “Transport of PacificWater Into the Canada Basin and the Formation of the Chukchi Slope Current,” J. Geophys. Res. Oceans, 2018.
[7] P. Stabeno, N. Kachel, C. Ladd, and R. Woodgate, “Flow Patterns in the Eastern Chukchi Sea: 2010–2015,” J. Geophys. Res. Oceans, 2018.
[8] M. Li, R. S. Pickart, M. A. Spall, T. J. Weingartner, P. Lin, G.W.K. Moore, and Y. Qi, “Circulation of the Chukchi Sea shelfbreak and slope from moored timeseries,” Prog Oceanogr. 172, 14–33, 2019.
[9] M. B. Porter and H. P. Bucker, “Gaussian beam tracing for computing ocean acoustic fields,” J. Acoust. Soc. Am. 82, 1349–1359, 1987.
[10] D. F. Gordon and H. P. Bucker, “Arctic acoustic propagation model with ice scattering,” Technical Report 985, Naval Ocean Systems Center, San Degio CA 92152, 1984.
[11] F. Fetterer, J. S. Stewart, and W. Meier, “MASAM2: Daily 4 km Arctic Sea Ice Concentration, Version 1,” (2015), updated daily.
[12] M. Siderius, M. B. Porter, P. Hursky, V. McDonald, and the KauaiEx Group, “Effects of ocean thermocline variability on noncoherent underwater acoustic Communications,” J. Acoust. Soc. Am., 121, 1895–1908, 2007.